FINAL REPORT

PROJECT I6

JANUARY 2024

Macroscopic Fundamental Diagram Estimation using Loop Detector Data

Jorge Laval, Ph.D., Georgia Institute of Technology
Zijian Ding, Doctoral Student, Georgia Institute of Technology
Garyoung Lee, Doctoral Student, Georgia Institute of Technology

STRIDE | Southeastern Transportation Research, Innovation, Development and Education Center

UF | Transportation Institute UNIVERSITY of FLORIDA

DISCLAIMER

The contents of this report reflect the views of the authors, who are responsible for the facts and the accuracy of the information presented herein. This document is disseminated in the interest of information exchange. The report is funded, partially or entirely, by a grant from the U.S. Department of Transportation's University Transportation Centers Program. However, the U.S. Government assumes no liability for the contents or use thereof.

ACKNOWLEDGEMENT OF SPONSORSHIP AND STAKEHOLDERS

We wish to acknowledge the generous sponsorship provided by the Southeastern Transportation Research, Innovation, Development, and Education Center (STRIDE) for supporting this work. Your contribution has been instrumental in advancing our research efforts, and we are grateful for your continued support in fostering innovation and development in the field of transportation.

Funding Agreement Number - 69A3551747104

LIST OF AUTHORS

Lead PI:

Jorge A. Laval, Professor
Georgia Institute of Technology, School of Civil and Environmental Engineering
Jorge.laval@ce.gatech.edu
ORCID 0000-0002-0986-4046

Additional Researchers:

Zijian Ding, Ph.D. student
Georgia Institute of Technology, School of Civil and Environmental Engineering
zding87@gatech.edu

Garyoung Lee, Ph.D. student
Georgia Institute of Technology, School of Civil and Environmental Engineering
garyounglee@gatech.edu

TABLE OF CONTENTS

LIST OF FIGURES

LIST OF TABLES

ABSTRACT

This project aims to examine the empirical estimation approach of the Macroscopic Fundamental Diagram (MFD) using loop detector data. The MFD give the network-wide relationship between average traffic variables and has become an invaluable tool for congestion management on large transportation networks. However, deriving the MFD using the empirical data is challenging since (i) the required loop detector data is not available in most of the cities, (ii) in the networks with available loop detector data, the loop detectors cover only a fraction of streets in the network, and (iii) the data coming from various loop detectors is prone to bias and inaccuracy, which makes the data cleaning and processing cumbersome. This project will rely on the recently published loop detector data from more than 40 cities over the globe and simulation experiments to investigate three main impacting factors on the network MFD: (i) the distribution of the loop detectors over the network, (ii) the distribution of loop detectors on the links, and (iii) the extent of the coverage area of the loop detectors and its relationship with the accuracy of the resulting MFD. As a result of this project, we aim to develop a robust method to accurately estimate the network MFDs considering the aforementioned impacting factors.

Keywords (up to 5):
Macroscopic fundamental diagram; Loop detector data; Traffic simulation

EXECUTIVE SUMMARY

Ever since cars came into existence, we have grappled with traffic congestion, a challenge that has grown even more significant today. Traditional link-level traffic control methods, while effective in certain scenarios, often become inefficient when applied in real-time to large networks. The Macroscopic Fundamental Diagram (MFD), which relates network-wide average traffic variables, emerges as a promising solution to this predicament. The MFD allows for the estimation of performance across all links within a network or zone through a single entity. This method not only simplifies the process but also cuts computational requirements.

However, fully realizing the MFD's potential is not without challenges. The accuracy and reliability of these estimations can be influenced by the measurement method, particularly the nature of loop detector. These detectors gather traffic data at specific installation points, potentially skewing the representation of the actual traffic state. Recognizing these challenges, this research project embarked on a mission to discover the impact of loop detector position on an empirical MFD estimation, as documented in the paper by Garyoung Lee, Zijian Ding, and Jorge Laval titled "Effects of loop detector position on the macroscopic fundamental diagram". The research explored the impact of loop detector positioning on MFD estimations through three approaches:

Analytical Approach: The study utilized a symmetric triangular fundamental diagram on a corridor to visualize potential biases induced by loop detectors. Under ideal signalization, no bias was evident. However, the loop detector MFD might not accurately represent link MFD in most of the cases, necessitating a correction method. Both the network's topology and the distribution of positions play a crucial role in this.

Empirical Analysis: Drawing from empirical loop detector data from 28 cities worldwide, termed UTD19, the analysis identified variations in installation parameters. Some scenarios exhibited no bias regardless of loop detector placements. Specific placements can potentially minimize MFD bias, i.e., more upstream with low variance .

Simulation Results: A microscopic simulation using SUMO on a 10x10 grid network revealed that MFD bias is also influenced by network parameters. Specifically, networks with shorter blocks are more susceptible to bias than those with longer blocks. In contrast, the aggregation interval did not affect MFD bias.

In summary, this research has significantly enriched our comprehension of the relationship between loop detector positioning and MFD estimation. The paper stands as a pivotal contribution from the research project, setting the stage for more accurate traffic control.

Reference:

Lee, G., Ding, Z., & Laval, J. (2023). Effects of loop detector position on the macroscopic fundamental diagram. Transportation Research Part C, 154.
https://doi.org/10.1016/j.trc.2023.104239

1.0 INTRODUCTION

Loop detectors are usually installed for traffic control and congestion monitoring. They typically report the traffic variables flow (i.e., number of vehicles passing a detector), and occupancy (i.e., share of time a detector is occupied). Loop detectors are mainly used for counting vehicles, detecting congestion, and controlling traffic signals. In the past few years, the loop detector data (LDD) has been used widely to estimate the network MFDs empirically since the empirical verification of existence of the MFD by Geroliminis and Daganzo (2008).

Different studies have shown that unpolished deployment of the LDD might negatively affect the MFD estimation due to (i) the detectors' distribution in the network, (ii) the detectors' location on the links, and (iii) the selected links for the set of equipped links. The first issue might result in more congested regime points, since the loop detectors are normally installed on the more congested links (Leclercq et al. 2014). The second issue might lead to the overestimation of the network average density when the detectors are installed closer to the downstream signals (Buisson and Ladier 2009, Ambühl et al. 2017), while the third issue might result in high-scattered MFDs (Keyvan-Ekbatani et al. 2013).

1.1 OBJECTIVE

The research objective of this project is to develop a robust method to estimate the MFD empirically using the available loop detector data, able to take into account the following impact factors:

(i) Distribution of loop detectors: the number and density of loop detectors in the network based on the area and topology of city. How the loop detectors are distributed over the network and how well they are sampling the links in the network.

(ii) Loop detector placement within the link: where the loop detectors are located on the link and how well they can capture the traffic conditions on the links, and

(iii) Coverage area: how the size of the area including the loop detectors can impact the shape and accuracy of the resulting MFD.

1.2 SCOPE

The current project will contribute to the empirical estimation of the MFD of the urban networks or zones inside the network using the available loop detector data by developing a robust empirical MFD estimation method not only by simply averaging the data from the loop detectors, but also by taking into account impacting factors such as the distribution of the loop detectors across the network and over the links, and the network partitioning and size of the resulting zones, which have not fully been investigated previously. As a result of this proposed method, the network or zone MFDs can be accurately estimated and then employed in the network control models.

2.0 LITERATURE REVIEW

The modeling of traffic flow dynamics in large urban networks has proven challenging over the years. An important branch of the efforts to control congestion is aggregated modeling. After Greenshields et al. (1935) observed for the first time the fundamental diagram of a single uninterrupted link, researchers took a profound interest in the aggregated relationship between average flow and density in entire urban signalized networks (Smeed, 1967; Mahmassani et al., 1984). The encapsulation of network traffic states into two variables is known as the Macroscopic Fundamental Diagram (MFD). Geroliminis and Daganzo (2008), and their empirical study in Yokohama, Japan demonstrated that the MFD is a convincing model to describe a network-level traffic performance. When aggregated at a network level, a high scatter of average flow and density from individual loop detectors nearly vanished and the points gather along the MFD curve.

Analytical, empirical, and simulation studies have been conducted to observe the MFD. Contemporaneous with Geroliminis and Daganzo (2008), Daganzo and Geroliminis (2008) presented the method of cuts (MoC) using variational theory (Daganzo, 2005) in a homogeneous signalized corridor, which sets the upper bound for the MFD. Stemmed from the literature, Geroliminis and Boyacı (2012) applied variational theory to parallel corridors with weak heterogeneity. Considering a strong heterogeneity of the real world, Laval and Castrillón (2015) proposed the stochastic MoC (SMoC) to handle networks with different block lengths and signal timings.

Numerous studies have verified that the MFD is applicable to other cities or arbitrary networks. In contrast to the findings from Geroliminis and Daganzo (2008) that the MFD is independent of demand, later researchers challenged that the finding is only apposite for homogeneous networks with low congestion levels which make a well-defined low-scatter MFD. Otherwise, the MFD reveals a trapezoidal shape and the hysteresis phenomenon with a high scatter (Geroliminis and Sun, 2011a,b). A host of posterior literature suggested that the MFD shape is dependent on demand (Mazloumian et al., 2010; Leclercq et al., 2015), network topology and heterogeneity (Zheng and Geroliminis, 2013; Geroliminis and Boyacı, 2012; Buisson and Ladier, 2009), routing strategy (Yildirimoglu et al., 2015; Ding et al., 2017), and signal control schemes (Gayah et al., 2014; Huang et al., 2018); see Zhang et al. (2020) for a more detailed summary of influential factors for MFDs.

While various exogenous influential factors of the MFD have been exhibited, the endogenous factor – the bias induced by the nature of empirical data – has not been discussed to a comparable extent. Loop detector data is arguably the most prevailing empirical source for exploring various facets of the MFD. Some studies use probe data, but even this is usually fused with loop detector data (Ji et al., 2014; Ambühl and Menendez, 2016; Du et al., 2016; An et al., 2020; Saffari et al., 2022). Although the loop detector is compelling as it measures traffic flow at all times, many have faced limitations in solely exploiting it reliably for various problems (Kong et al., 2009b; Kim et al., 2020; Min et al., 2022). Consequently, researchers have been striving

to mitigate the inherently noisy property of loop detector data (Bramich et al., 2023) or to seek alternative sensing technologies, such as unmanned aerial vehicles (Barmpounakis and Geroliminis, 2020; Paipuri et al., 2021), as a means to estimate the MFD without relying on loop detector data. Among the issues encountered with loop detectors, its installation position along the link is found to be critical for the accurate representation of traffic flow.

However, the engineering installation standards for urban areas seem not to prioritize the issue of traffic state representation accuracy (FHWA, 2022). Their primary purpose lies in the effective control of traffic signals: e.g., left-turn queue detection for the actuated control and the conventional adaptive signal control technologies such as SCOOT1 (Hunt et al., 1981), SCATS2 (Sims, 1979), and RHODES3 (Mirchandani and Head, 2001). For instance, Kay et al. (1975) recommends the minimum distances for longitudinal placement range from 61 to 76.2 meters from the upstream intersection stop line with the comprehensive consideration of cycle length, split, and offset. The detector placements under SCOOT, SCATS, and RHODES policy tend to be constant across the network, either all placed at the same distance from the downstream or at the stop bar (Moore II et al., 1999; Kong et al., 2009a; FDOT, 2016). While effective for signal control, the literature casts doubt on the detectors' ability to the network-level representativeness of traffic flow and density by their position distributions.

Buisson and Ladier (2009) first realized that the position of the loop detectors within the links plays a substantial role in defining the MFD shape. They split the measurements from the detectors in Toulouse, France into three subsets according to the physical distance to the downstream traffic signal. Closer to the signal, the free-flow branch of MFD showed a lower slope. The overestimation of the queue stood as the rationale. Using simulation, Courbon and Leclercq (2011) compared three positionings-constant, uniformly distributed, and normally distributed – of virtual detectors on a corridor with an identical block length. Although the constant distance setting displayed the largest bias, the detectors farther from the downstream signal reproduced the free-flow conditions well and the closer ones reproduced the queues well at the cost of the lower slope of the free-flow branch. Uniform distribution of the detectors showed the most accurate fit to the MoC. Leclercq et al. (2014) proved that the uniform distribution of detectors is also the best strategy for the homogeneous network to reproduce accurate traffic state. Ambühl et al. (2017) leveraged this finding to explain not only the discrepancy in the MFD drawn by the loop detector and floating car data from Zurich, Switzerland, but also the decreased average occupancy when the detectors closer to the downstream signal were excluded. They pointed out that the loop detector bias owes to the non-uniform placement and the link selection: the detectors are mostly placed at the beginning or the end of the link, and they are installed in certain links to control traffic signals and congestion.

Although previous literature showed how the loop detector positions influence the shape of MFD and why the bias happens, still there are important gaps to be filled. First, two different biases induced by the nature of detectors are distinguished here: (i) the bias between the link

MFD and the loop detector (LD)-MFD (henceforth, LD bias) and (ii) the bias between position-based subsets of LD-MFD (henceforth, subset bias). Note that the link MFD can be thought of as the ''ground-truth'' as it gives Edie's generalized traffic state definitions (Edie et al., 1963). The subset bias refers to MFDs using detectors that belong to a particular location subset: upstream, midstream or downstream within the link. Notice that Courbon and Leclercq (2011) and Buisson and Ladier (2009) concluded that the detector position affects the MFD without distinguishing these two biases although what they measured turned out to be LD bias and subset bias, respectively. Second, identifying network characteristics that contribute to each bias is required since the literature used only a single network when explaining the existence of bias. Third, even though the uniform distribution of the positions is proved to be the best strategy (Courbon and Leclercq, 2011; Leclercq et al., 2014), we need a further investigation on how an arbitrary distribution of detector positions affects the MFD. Lastly, as mentioned in Ambühl et al. (2017), the variability of block lengths and the spatial density across the network should be taken into consideration.

3.0 METHODOLOGY or TASK(s)

To accomplish the research objectives of this proposal we will carry out the following tasks.

Task 1: Literature Review

Our existing background research will be extended in more detail and expanded to incorporate the latest research in the fields of network MFD and associated estimation methods.

Task 2: Data assembly and preparation

At the heart of this proposal is the compilation of additional empirical MFD data. Two main sources of data will be used in this research project: (i) the empirical loop-detector data provided by UTD-19 (Loder et al. 2019) and (ii) other open source dataset from published research articles. The UTD19 dataset is collected by a research group from ETH Zurich in the period of 2017-2019 and is "a large-scale traffic dataset from over 23541 stationary detectors on urban roads in 40 cities worldwide making it the largest multi-city traffic dataset publicly available"

After careful analysis of the data quality, a subset of cities will be selected for further data collection. For these cities, additional data will be collected, such as the underlying transportation network (from Google earth and Open Street maps), average signal timing settings, and bus operation characteristics (from the appropriate traffic management authorities).

Task 3: Analytical and simulation models

In parallel to Task 2, analytical models will be developed to predict the impacts in the MFD of the 3 factors above (number, placement, and coverage area of detectors). These models will be

based on simplifying assumptions for tractability, and should reveal important qualitative insights about the problem.

In addition, a microscopic network simulation environment in SUMO will be set up using the loop detector information and GIS information of the transportation network. The microscopic network simulation will be used to reproduce the empirical MFDs and verify and generalize our analytical results.

Task 4: Improved MFD estimation method

this is the main task of the project, where the empirical data, analytical models and microscopic network simulations will be combined to produce an improved MFD estimation method. For the cities selected for further analysis in Task 2, the following steps will be followed to analyze the impact of detector placements:

(i) network simulation models will be set up to reproduce the empirical observations,

(ii) "ground truth" MFD: the network simulation models will be modified to report the actual traffic states on whole links (rather than the traffic state measured by the virtual loop detector at its specific location)

(iii) The analytical insights derived in Task 3 will be used to come up with the simplest possible method to reconcile the ground truth MFD with the empirical MFD. It is expected that the method will modify the empirical data at each loop detector based on the placement of the detector within the link, but several other methods will be analyzed.

4.0 RESULTS

4.1 Analytical corridor approximation

Recall that the LD bias refers to the bias between the link MFD and the LD-MFD and the subset bias refers to the bias between position-based subsets of LD-MFD. In this section, we assume a homogeneous corridor that obeys a symmetric triangular fundamental diagram (FD) to analyze LD bias and subset bias. As customary to simplify the analysis, we will use isosceles fundamental diagrams (free-flow speed = wave speed) since one obtains the same solutions using a general triangular FD (Laval and Castrillón, 2015; Laval and Chilukuri, 2016).

Table 1 Descriptions of constants and variables. Note that the symbols with asterisks are constants, and otherwise, variables.

Traffic states		Physical attributes of the network	
O	Void state*	l	Link length
A	Current state	N	The number of links*
C	Capacity state*	N_u	The number of links with loop detector located upstream of critical position
J	Jam state*	N_d	The number of links with loop detector located downstream of critical position
Fundamental Diagram		**Signal Setting**	
u	Free-flow speed*	R	Red signal time
w	Wave speed*	G	Green signal time
s	Shock wave speed	n	Ceiling of time in unit of cycle length for 1st vehicle in green arrives at next intersection
k_c	Critical density*	**Dimensionless parameter**	
Q	Capacity*	λ	Link length to critical link length ratio ($= \frac{l}{l^*}$)
		ρ	Red time to green time ratio ($= \frac{R}{G}$)

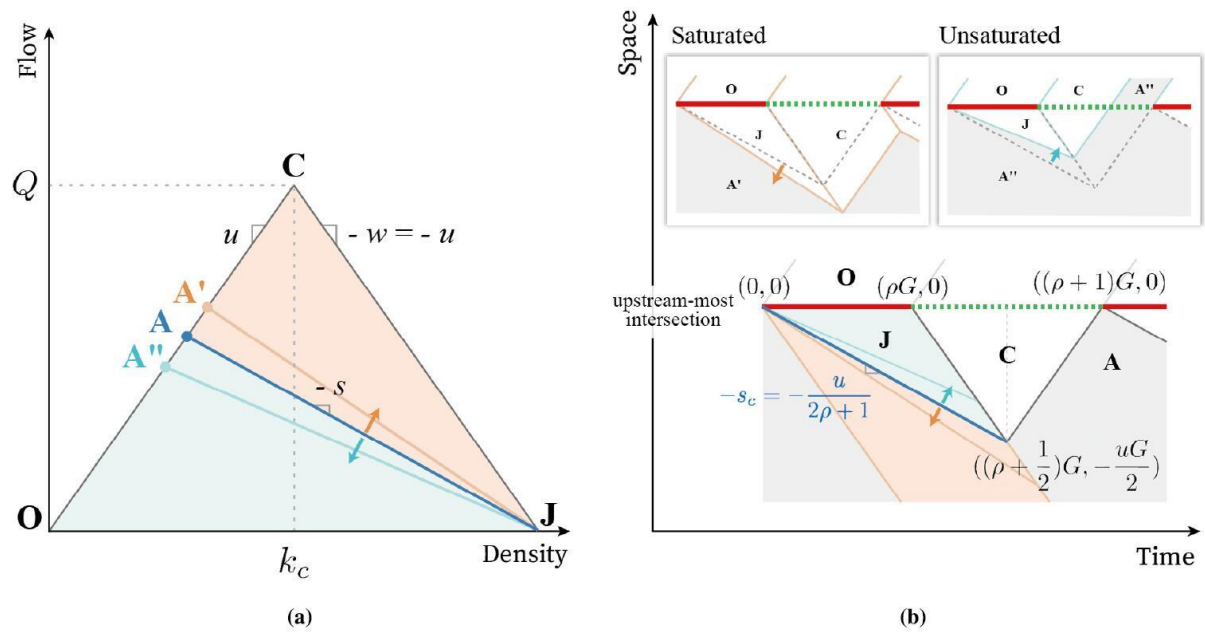

Fig 1 Initial conditions: (a) A fundamental diagram with different shock waves; (b) Time-space diagrams of the saturated and unsaturated condition.

The corridor to be analyzed consists of N links with an identical block length of l. The traffic signal on all intersections is fixed with green time, G, and red time, R, with no offset. The symmetric triangular FD has a free-flow speed of u, a critical density of kc, and a capacity of Q. As shown in Fig. 1(a) the queue initially grows at a shock wave speed s in the upstream-most intersection, depicted as a state **A**, and clears at a wave speed w. The traffic state of zero flow with zero density, $i.e.$, a void, is depicted as a state **O**. The traffic state of the capacity and the jam density are each denoted as state **C** and state **J**, respectively. The variables and constants used are summarized in Table 1. Note that the symbols with asterisks are constants, and otherwise, variables.

Here, it is important to introduce two dimensionless parameters, the mean block length to critical length ratio, λ, and the mean red signal time to mean green signal time, ρ, which

significantly influence the MFD shape according to Laval and Castrillón (2015). The critical length, l, corresponds to the minimum block length that prevents spillbacks. Then λ is expressed as:

$$\lambda = \frac{l}{l^*} = \frac{l}{G/(\frac{1}{u}+\frac{1}{\omega})} = \frac{l}{G/(\frac{2}{u})} = \frac{2l}{uG} \tag{1}$$

Under the given settings, all possible patterns of the time-space diagram can be categorized according to four variables: (i) s, (ii) λ, (iii) ρ, and (iv) n. First of all, the shock wave speed becomes the primary determinant. It decides whether the initial condition influences the downstream links. The critical state $\mathbf{A}$ and the corresponding critical shock wave, s_c , are obtained where the queue clearance wave intersects the end of the green phase (Fig. 1(b)). Thus, the critical shock wave speed is the slope between the origin and the queue dissipation point, $s_c = \frac{u}{2\rho+1}$. If the shock wave speed is steeper than the critical shock wave speed (state $\mathbf{A}'$), the first queue clearance wave is obstructed by the queue of the next red phase. This conveys that the queue accumulated in the red signal phase loses a chance to completely vanish before the next cycle. On the other hand, if the shock wave speed is lower (state $\mathbf{A}''$), the queue clearance wave traverses through the green phase, causing the initial state $\mathbf{A}''$ to spread to the downstream link. Hereafter, the initial condition that exceeds or equals the critical shock wave speed is considered a saturated initial condition, otherwise an unsaturated. Under saturated conditions, the time-space diagram of the upstream-most intersection is duplicated at downstream links, while unsaturated initial conditions do not provide this guarantee. The uncertainty of the repetition ascribes to the spread of the initial state to the downstream links. This causes some cases of unsaturated initial condition to not be expressed in a closed form. Hence, we only address the saturated condition in the following.

Fig. 2. depicts all possible types of time-space diagrams in the saturated initial condition. It is confirmed for all three cases that the traffic state patterns recur throughout the corridor, by extending the time-space diagrams to an infinite homogeneous corridor. Importantly, the existence of the jam state and the coverage of the void state distinguish three cases. As indicated by a blue line, the difference originates from the time it takes for the first vehicle in a green phase to reach the next intersection.

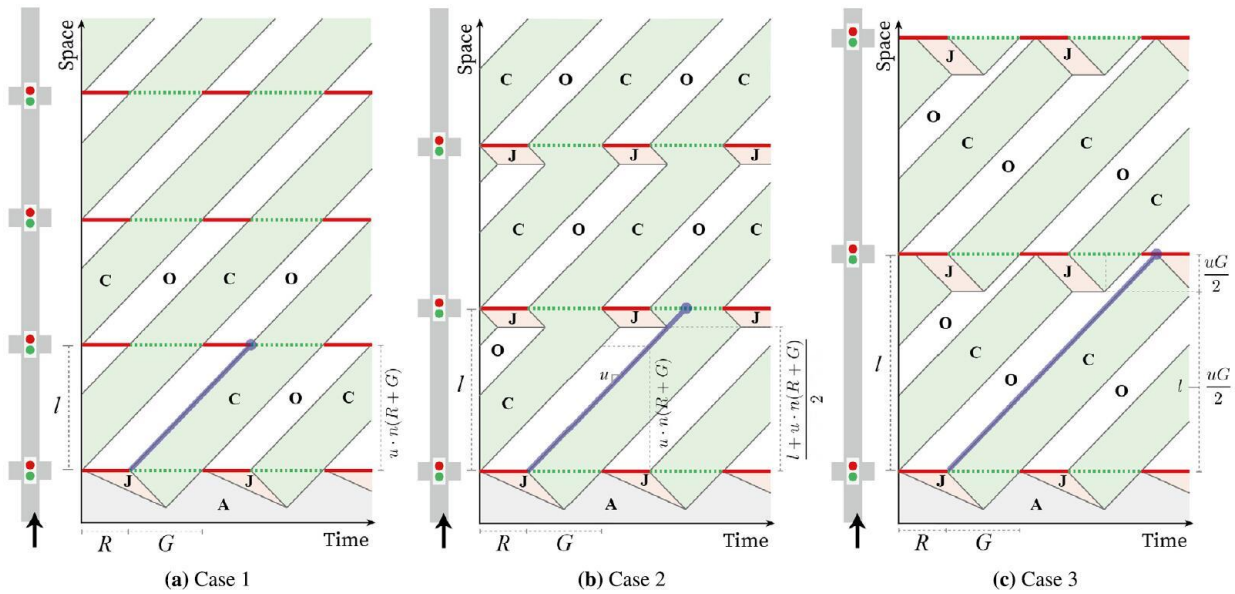

Fig 2 Three types of time-space diagram at the saturated initial condition.

A method to derive the MFD from the time-space diagram is explained in the following. Note that only the downstream links of the upstream-most intersection are considered. We assume all N links have one detector installed on each, and the aggregation interval is a multiple of a cycle length. This enables setting the aggregation interval simply as a cycle length. In order to obtain the LD-MFD, firstly, draw a horizontal line on a time-space diagram at the position of a detector by the amount of the aggregation interval. Second, calculate the weighted average of the traffic state, $i.e.$, a pair of density-flow, using the time proportion of each state as a weight. This corresponds to the FD of a detector, which is then a linear combination of traffic states $\mathbf{O}$, $\mathbf{C}$, and $\mathbf{J}$. Lastly, for every time interval measured, average the density-flow pair of all detectors to obtain the LD-MFD (Eq. (2)). While the LD-MFD uses the proportion of time as a weight, the link MFD can be obtained by using the proportion of the area of each traffic state throughout the link as a weight. The link MFD in the saturated initial condition equals to the intersection point where the stationary cut and the forward cut of MoC.

$$q_{LD} = \frac{\sum_i q_i l_i}{\sum_i l_i}, k_{LD} = \frac{\sum_i k_i l_i}{\sum_i l_i} \tag{2}$$

whereq_{LD} is the average flow, k_{LD} is the average density, and q_i and k_i are the flow and density measured by the loop detector i of installed link length of l_i . The MFD for each case through the above process is summarized in Table 2. We now disentangle the constraints and MFD formulae; i.e., how λ, ρ, and n act as the keys to distinguish these three.

1. Case 1: No queues

According to Fig. 2(a), the first vehicle of the green phase never encounters the red phase and so do all other vehicles. Notice that only the void and the capacity state exist. This is only possible when the time for the vehicle to complete passing the link is equal to a multiple of a cycle length. This constraint is simplified using definitions of λ and ρ as follows:

$$\frac{l}{u} = n(R + G) \tag{3a}$$

$$\lambda = 2n(\rho + 1) \tag{3b}$$

Since the traffic states are homogeneous along the link, MFD is not subject to any bias no matter where the detector is positioned. In any of the positions during a cycle $R + G$, the void state $\mathbf{O}$ and the capacity state $\mathbf{C}$ are measured by the amount of the red time R and the green time G, respectively. Thus, the FD of all loop detectors correspond to $\frac{\rho}{1+\rho} \cdot \mathrm{O} + \frac{1}{1+\rho} \cdot \mathrm{C} + 0 \cdot \mathrm{J}$, so do the MFD.

2. Case 2: Jam exists & voids are finite

Compared to Case 1, Fig. 2(b) bares the jam state for a certain length. The jam accumulates because some vehicles departed at a previous intersection cannot pass the intersection ahead being blocked by the red time. This happens when the first vehicle of the green time was able to pass the next intersection without stopping but was not the foremost vehicle passed during its green time. That is, the time for the first vehicle to arrive at the next intersection is a multiple of a cycle length plus a partial or a full amount of green time. This condition is formulated as below:

$$n(R + G) < \frac{l}{u} \leq n(R + G) + G \tag{4a}$$

$$2n(\rho + 1) < \lambda \leq 2n(\rho + 1) + 2 \tag{4b}$$

As traffic states are non-homogeneous along the link, identifying the critical position that turns the void state into the jam state is necessary. Separating the travel time into a multiple of a cycle length and the remainder gives us the length of the jam state. The distance vehicle traveled during n-multiple of cycle length is $u \cdot n(R + G)$. The remaining distance of $l - u \cdot n(R + G)$ is bisected by the void state and the jam state due to the symmetry of the FD. Then, the length of jam state and the void state are $(l - u \cdot n(R + G)) / 2$ and $(l + u \cdot n(R + G)) / 2$, respectively. If the loop detector is installed downstream of the critical position, the jam state $\mathbf{J}$ and the capacity state $\mathbf{C}$ will be each measured for the red time R and the green time G during an aggregation interval $(R + G)$. On the other hand, if the detector is installed at upstream of the critical position, the red time and the green time are each occupied by the void state $\mathbf{O}$ and the capacity state $\mathbf{C}$. With specifying that Nd and Nu detectors are installed at each downstream and upstream of critical position, the LD-MFD will have a linear combination of:

$$\frac{\rho}{1+\rho} \cdot \frac{N_d}{N_u+N_d} \cdot \mathrm{O} + \frac{1}{1+\rho} \cdot \mathrm{C} + \frac{\rho}{1+\rho} \cdot \frac{N_d}{N_u+N_d} \cdot \mathrm{J} \tag{5}$$

Here, the bias of LD-MFD is unavoidable unless the number of detectors in each position label is proportional to its length: $i.e.$, $N_d \propto (l - u \cdot n(R+G)) / 2$ and $N_u \propto (l + u \cdot n(R+G)) / 2$. Namely, the link MFD, which is theoretically a weighted average of each traffic state's area, can be simply calculated by substituting corresponding lengths to the number of detectors. Similar to Buisson and Ladier (2009), partitioning the loop detectors by their position gives us the position-based subsets of the MFD. For example, the downstream subset can be obtained by substituting N_d = 1 and N_u = 0 to the LD-MFD. The corresponding MFD expressions can be found in Fig. 2.

3. Case 3: Jam exists & voids are infinite

Compared to Case 2, jam is accumulated for a shorter period of time and the void fills the gap (Fig. 2(c)). The red time is already initiated before the first vehicle of the green time arrives at the next intersection. The amount of red time elapsed before the jam accumulation remains as the void. This is only available when the link travel time of the vehicle equals a multiple of a cycle length plus a full green time plus a partial red time, as below.

$$n(R+G) + G < \frac{l}{u} < n(R+G) + G + R \tag{6a}$$

$$2n(\rho+1) + 2 < \lambda < 2(n+1)(\rho+1) \tag{6b}$$

The critical position is obtained by the relationship between the free-flow speed u and the queue clearance duration G. Using that the jam always dissipates exactly before the red phase begins, the spatial length of the jam state is $u \cdot G / 2$. The loop detectors located downstream of the critical position will measure the void state $\mathbf{O}$ for time $\frac{l}{u} - n(R+G) - G$, the capacity state $\mathbf{C}$ for green time G, and the jam state $\mathbf{J}$ for the rest of a cycle. At the upstream of the critical position, the void state $\mathbf{O}$ and the capacity state $\mathbf{C}$ are observed by the amount of red time R and the green time G, respectively. With the assumption of the number of detectors N_d

and N_u , the weighted average gives LD-MFD. The link MFD and the position-based subsets are calculated likewise to Case 2 and one can refer to Table 2.

Table 2 Summary of link MFD, LD-MFD, and position-based subsets.

Case 1: $\lambda = 2n\ (\rho+1), \quad n = 0, 1, 2, \cdots$			The proportion of time during a cycle		
LD position	Length	Detector count	$\mathbf{O}\ (0,0)$	$\mathbf{C}\ (k_c, Q)$	$\mathbf{J}\ (2k_c, 0)$
-	l	N	$\frac{R}{R+G} = \frac{\rho}{1+\rho}$	$\frac{G}{R+G} = \frac{1}{1+\rho}$	0
MFD (LD = Link)	Linear combination	$\frac{\rho}{1+\rho} \cdot \mathbf{O} + \frac{1}{1+\rho} \cdot \mathbf{C} + 0 \cdot \mathbf{J}$			
	Coordinate	$\left(\frac{1}{1+\rho} k_c, \quad \frac{1}{1+\rho} Q\right)$			
Case 2: $2n\ (\rho+1) < \lambda \leq 2n\ (\rho+1) + 2, \quad n = 0, 1, 2, \cdots$			The proportion of time during a cycle		
LD position	Length	Detector count	$\mathbf{O}\ (0,0)$	$\mathbf{C}\ (k_c, Q)$	$\mathbf{J}\ (2k_c, 0)$
Downstream of critical position	$\frac{l-u \cdot n(R+G)}{2} = \frac{uG}{2}\left(\frac{\lambda}{2} - (1+\rho)n\right)$	N_d	0	$\frac{G}{R+G} = \frac{1}{1+\rho}$	$\frac{R}{R+G} = \frac{\rho}{1+\rho}$
Upstream of critical position	$\frac{l+u \cdot n(R+G)}{2} = \frac{uG}{2}\left(\frac{\lambda}{2} + (1+\rho)n\right)$	N_u	$\frac{R}{R+G} = \frac{\rho}{1+\rho}$	$\frac{G}{R+G} = \frac{1}{1+\rho}$	0
LD-MFD	Linear combination	$\frac{\rho}{1+\rho} \cdot \frac{N_u}{N_u+N_d} \cdot \mathbf{O} + \frac{1}{1+\rho} \cdot \mathbf{C} + \frac{\rho}{1+\rho} \cdot \frac{N_d}{N_u+N_d} \cdot \mathbf{J}$			
	Coordinate	$\left(\frac{1}{1+\rho}\left(1 + 2\rho \frac{N_d}{N_u+N_d}\right) k_c, \quad \frac{1}{1+\rho} Q\right)$			
Link MFD	Linear combination	$\frac{\rho}{1+\rho} \cdot \left(\frac{1}{2} + \frac{1+\rho}{\lambda} n\right) \cdot \mathbf{O} + \frac{1}{1+\rho} \cdot \mathbf{C} + \frac{\rho}{1+\rho} \cdot \left(\frac{1}{2} - \frac{1+\rho}{\lambda} n\right) \cdot \mathbf{J}$			
	Coordinate	$\left(\left(1 - \frac{2\rho}{\lambda} n\right) k_c, \quad \frac{1}{1+\rho} Q\right)$			
Position-based subset LD-MFD	Coordinate	Downstream: $\left(\frac{1+2\rho}{1+\rho} k_c, \frac{1}{1+\rho} Q\right)$ Upstream: $\left(\frac{1}{1+\rho} k_c, \frac{1}{1+\rho} Q\right)$			
Case 3: $2n\ (\rho+1) + 2 < \lambda < 2(n+1)(\rho+1), \quad n = 0, 1, 2, \cdots$			The proportion of time during a cycle		
LD position	Length	Detector count	$\mathbf{O}\ (0,0)$	$\mathbf{C}\ (k_c, Q)$	$\mathbf{J}\ (2k_c, 0)$
Downstream of critical position	$\frac{uG}{2} = \frac{l}{\lambda}$	N_d	$\frac{\frac{l}{u} - n(R+G) - G}{R+G} = \frac{\lambda-2}{2(1+\rho)} - n$	$\frac{G}{R+G} = \frac{1}{1+\rho}$	$\frac{(n+1)(R+G) - \frac{l}{u}}{R+G} = n + 1 - \frac{\lambda}{2(\rho+1)}$
Upstream of critical position	$l - \frac{uG}{2} = l\ (1 - \frac{1}{\lambda})$	N_u	$\frac{R}{(R+G)} = \frac{\rho}{1+\rho}$	$\frac{G}{R+G} = \frac{1}{1+\rho}$	0
LD-MFD	Linear combination	$\frac{\left(\frac{\lambda-2}{2(1+\rho)} - n\right) \cdot N_d + \frac{\rho}{1+\rho} \cdot N_u}{N_u+N_d} \cdot \mathbf{O} + \frac{1}{1+\rho} \cdot \mathbf{C} + \left(n + 1 - \frac{\lambda}{2(1+\rho)}\right) \cdot \frac{N_d}{N_u+N_d} \cdot \mathbf{J}$			
	Coordinate	$\left(\left(\frac{1}{1+\rho} + \left(n + 1 - \frac{\lambda}{2(1+\rho)}\right) \frac{2N_d}{N_u+N_d}\right) k_c, \quad \frac{1}{1+\rho} Q\right)$			
Link MFD	Linear combination	$\left(\frac{1+2\rho}{2(1+\rho)} - \frac{n+1}{\lambda}\right) \cdot \mathbf{O} + \frac{1}{1+\rho} \cdot \mathbf{C} + \left(n + 1 - \frac{1}{2(1+\rho)}\right) \cdot \mathbf{J}$			
	Coordinate	$\left(\frac{2(n+1)}{\lambda} k_c, \quad \frac{1}{1+\rho} Q\right)$			
Position-based subset LD-MFD	Coordinate	Downstream: $\left(\left(\frac{1-\lambda}{1+\rho} + 2(n+1)\right) k_c, \frac{1}{1+\rho} Q\right)$ Upstream: $\left(\frac{1}{1+\rho} k_c, \frac{1}{1+\rho} Q\right)$			

4.2.2 Discussions on subset bias and LD bias

Figs. 3 and 4 illustrate MFD realizations of the corridors with different network parameters. The FD is drawn at the back for comparison with the MFDs. Case 1 shows that neither the LD bias nor the subset bias resides in the MFD since the corridor has an ideal signal setting that the queue never forms (Fig. 3(a)). Regardless of n and λ, the MFD of a corridor always lies exactly on the free-flow branch of FD and only moves along the branch depending on the ρ. Specifically, the yellow–green dot displayed a much slower critical shock wave speed and a smaller average density than the blue dot due to its higher ρ value. This means that insofar as two different corridors have the same ρ value, their MFDs stand identical regardless of different n.

Unlike Case 1, differences between MFDs can be discerned in the remaining cases. The link MFD, LD-MFD, upstream subset, and downstream subset are labeled with a solid circle, grey-filled symbols, open circle, and open square, respectively. Slopes that connect the origin and

the points of MFD are considered free-flow branches of the corresponding MFD. The shaded area shows the possible range between the upstream and downstream subsets to which the free-flow branch of LD-MFD can fall on. The dotted line will be the range of the exact point of LD-MFD that can be placed. In the saturated initial condition, the bias takes place only in average density values. Despite the cases, the average flow is always $\frac{1}{1+\rho}\boldsymbol{Q}$, which is consistent with the stationary cut of MoC (Daganzo and Geroliminis, 2008). Calculations reveal that the link MFD corresponds to the point where the stationary cut and the forward cut intersect regardless of parameters and cases (Fig. 4(a)).

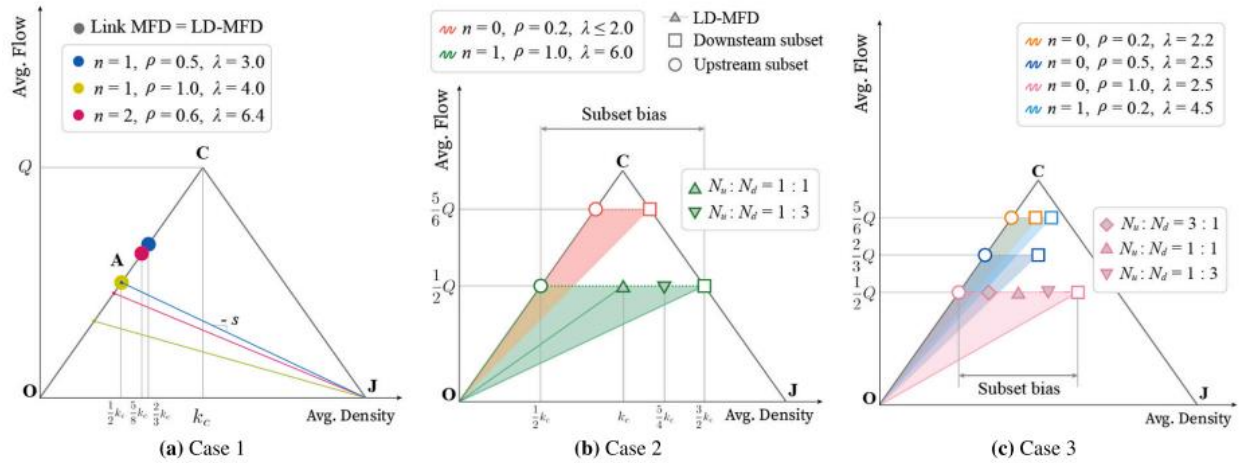

Fig 3 Case 1 with no bias and the representation of the subset bias on Cases 2 and 3

1. Subset bias

We can identify the subset bias through the difference between position-based subsets, i.e., the downstream subset and the upstream subset; see Figs. 3(b) and 3(c). Regardless of the loop detector distribution, the upstream and downstream subset is determined by the network parameters; see green and pink LD-MFDs. It is prominent that the downstream subset underestimates the average free-flow speed while the upstream subset overestimates it. In our analytical approximation setting, the downstream subset holds the key to determining the subset bias, as the slope of the upstream subset is always fixed with the free-flow speed of FD, u.

In Case 2, the downstream subsets fall exactly on the congestion branch of FD regardless of the parameters. The magnitude of the subset bias, which is $\frac{2\rho}{1+\rho}\boldsymbol{k_c}$with respect to the average density, is determined only by the value of ρ. Larger ρ decreases the maximum average flow and increases the subset bias, i.e., green area (ρ = 1) is larger than the red (ρ = 0.1). This means that the subset bias is inevitable unless ρ is negligibly small.

In Case 3, the downstream subsets do not lie on the congestion branch. As the subset bias with respect to the average density equals $\left(\boldsymbol{2(n+1)}-\frac{\boldsymbol{2\rho}}{\boldsymbol{1+\rho}}\right)\boldsymbol{k_c}$, the subset bias gets smaller when λ approximates the right-hand side of the constraint of Case 3 (Eq. (6b)). This is because the corridor becomes more free-of-congestion with the approximation of λ. We can also notice that

(i) identical ρ does not guarantee the same subset bias, i.e, cyan $\neq$ orange and (ii) larger ρ does guarantee neither a larger subset bias nor a linear increment by ρ.

2. LD bias

LD bias is clearly recognizable by the green and pink symbols in each Figs. 4(b) and 4(c), i.e, the difference between the circle symbol and the grey-filled symbol. While the link MFD is fixed according to the network parameters, LD-MFDs can take place anywhere between the upstream and downstream subsets depending on the distribution of detectors. The link MFD is generally closer to the upstream subset than the downstream subset under this setting because the length of the jam state is shorter than half of the link length. LD bias will converge to zero when the number of detectors of each position is proportional to its length: e.g.,$\boldsymbol{N_d} \propto (l - u \cdot n(R + G)) / 2$ and $\boldsymbol{N_u} \propto (l + u \cdot n(R + G)) / 2$ for Case 2. This validates the findings from Courbon and Leclercq (2011) that the uniform distribution of the detectors across the corridor can best emulate the MoC.

Since the range to which LD-MFDs and link MFDs can exist is equal to subset bias, the estimation of subset bias helps conjecture the maximum amount of LD bias. In terms of Case 2, the size of the range of LD-MFD with respect to the average density is $\frac{\boldsymbol{2\rho}}{\boldsymbol{1+\rho}}\boldsymbol{k_c}$. The range increases as ρ increases, which might lead to a higher LD bias. Insofar as two corridors have the same ρ such as red and yellow symbols, the position-based subsets, i.e., the maximum amount of LD bias, are identical despite different link MFDs. When having the same ρ value, the possible range of LD-MFD is shorter in Case 3 than in Case 2. This is because the LD bias of Case 3 is affected by λ, ρ, and n. Especially for Case 3, the possible ranges of LD-MFD of two corridors with equal n and λ are proportional to the rate of ρ.

3. Remarks of analytical corridor approximation

In this section, we adopted a symmetric triangular FD in a homogeneous corridor to distinguish and give a credence to the existence of LD bias and subset bias. Under the saturated initial condition, subset bias is inevitable unless the traffic signal system (i) is perfect that never forms a queue (Case 1) or (ii) has a negligibly small red time portion under Case 2, or (iii) satisfies diminutive $2(n + 1) - \lambda / (1 + \rho)$ under Case 3. We also identified that the position-based subsets are determined by the network parameters, λ, ρ and n. Note that detectors must be installed on all links for subsets to be dependent only on the network structure.

Additionally, we reinterpreted that the uniform distribution of the detectors across the corridor assures the non-existence of LD bias. However, the LD bias occurs unless the signal timing is perfectly programmed as Case 1. This implies that it will be rare for the LD-MFD not to be biased in real world. Despite the importance of accurate traffic state representation, we may never know the link MFD unless we have an almighty information about the network. When LD bias is directly immeasurable, we propose that the subset bias can be used to estimate the maximum amount of LD bias. In a fortunate case, a negligible subset bias will allow us to conclude that the LD-MFD is unbiased. Otherwise, the existence of subset bias cautions users to

carefully rely on the data as it may not represent the traffic state at an aggregated network level.

As the findings are identified even in a simplest and tractable setting of a triangular FD, other renowned FD models can be used to show the same implications; i.e., the LD bias exists, the downstream and upstream subset is each minimum and maximum of link MFD, and thus the subset bias can be used to estimate the possible range of LD bias. For applicable compendium of models, readers are referred to Bramich et al. (2022).

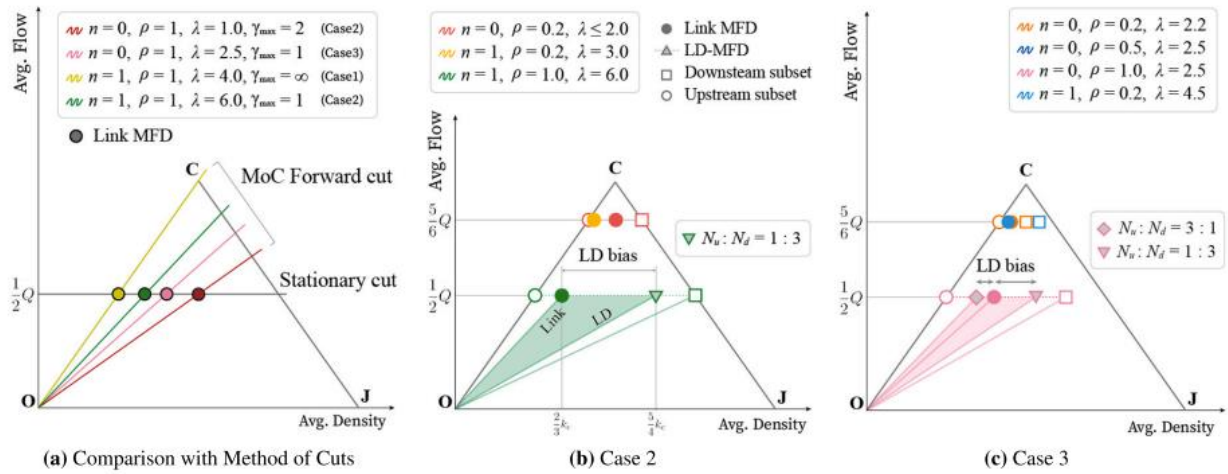

Fig 4 The implication of Link MFD and the representation of the LD bias (Note: Link MFD is always identical to the intersection of the MoC forward cut and stationary cut.)

4.2. Simulation results

We have taken both signal and network settings into account figuring out the influential factor of the MFD shape, by changing λ. Fig. 3 illustrates the MFDs of four networks with different λ and the aggregation interval of 3 minutes. The average flow and the density are each normalized by the value of Q and $\boldsymbol{k_j}$, respectively. Note that the free-flow speed and the wave speed of FD are each 4.3 and 1.3 when normalized. The forward cuts of the MoC and the SMoC calculated through the parameters of each network are also superimposed.

We can verify that the random positioning within the position range does not hinder the accurate representation of the link MFD since the link MFD and LD-MFD aligns well on all four figures. Also, it is observed that the link MFD is well bounded by the forward cuts of the MoC and the SMoC. As discussed in both previous sections, free-flow branch slopes are high by order of upstream, midstream, and downstream subsets. In view of a congested branch, the downstream subset overestimates its slope and the upstream subset underestimates it. Hence, from the viewpoint of subset bias, the downstream and upstream subsets show each left-skew and right-skew distribution from the link MFD. We have explicitly shown that the upstream subset is not bounded by the forward cut. The midstream subsets of all four figures are considerably close to the upstream subset, meaning that the jam state is not likely to propagate beyond the third downstream point. Following are the main observations as λ increases.

• The maximum average flow increases since the long blocks are not prone to spillbacks. This is consistent with the findings from Zhang et al. (2013) that the shorter blocks tend to have a lower maximum flow rate.

• It is observed that free-flow branches of other MFDs including the link MFD approach that of the upstream subset. The free-flow branch of the upstream subset also gets steeper and closer to the free-flow speed $\boldsymbol{u_f}$. This implies that the duration of the traffic jam is canceled out by the long block length.

• Larger λ assures the smaller subset bias. While the free-flow branches highly differ by the subsets in shorter blocks, these become overlapped as λ increases. Recalling that we have stated that the possible range of LD bias is equivalent to the subset bias, longer blocks have less chance to show bias in the LD-MFD.

• This is also analytically demonstrated by the slope of MoC and SMoC forward cut (Table 3). The average speed of the observer passing the origin increases when λ gets larger. Namely, the difference between the free-flow slope of the upstream subset and the slope of forward cuts becomes smaller. For long blocks, $umax$ approximates the free-flow speed $\boldsymbol{u_f}$. However, in short blocks, $umax$ is just half of the free-flow speed (see Fig. 3).

Table 3 The forward cut parameters of the MoC and the SMoC. Note that $\boldsymbol{\gamma_{max}}$ and $\boldsymbol{u_{max}}$ are the number of blocks that the observer with free-flow speed can pass without stopping and the average speed of the observer in the forward cut passing the origin, respectively. $\boldsymbol{u^{\#}_{s_1}}$ and $\boldsymbol{u^{\#}_{s_2}}$ are the average speed of the observer in SMoC, each corresponds to the steepest forward cut and the next steepest forward cut. Also note that $c = (1 + \boldsymbol{\delta^2})\, \boldsymbol{\rho^2}/(\lambda(1 + \rho))$.

Variables		$\lambda = 0.5$	$\lambda = 1$	$\lambda = 2$	$\lambda = 4$
Method of Cuts	γ_{max}	9	5	3	2
	u_{max} (km/h)	**27**	**32.04**	**38.16**	**51.84**
	u_{max} (normalized)	2.15	2.55	3.04	4.13
Stochastic Method of Cuts	c	1	0.5	0.25	0.125
	$u^{\#}_{s_1}$	2	2.67	3.2	3.55
	$u^{\#}_{s_2}$	0.6	0.83	1.125	1.42

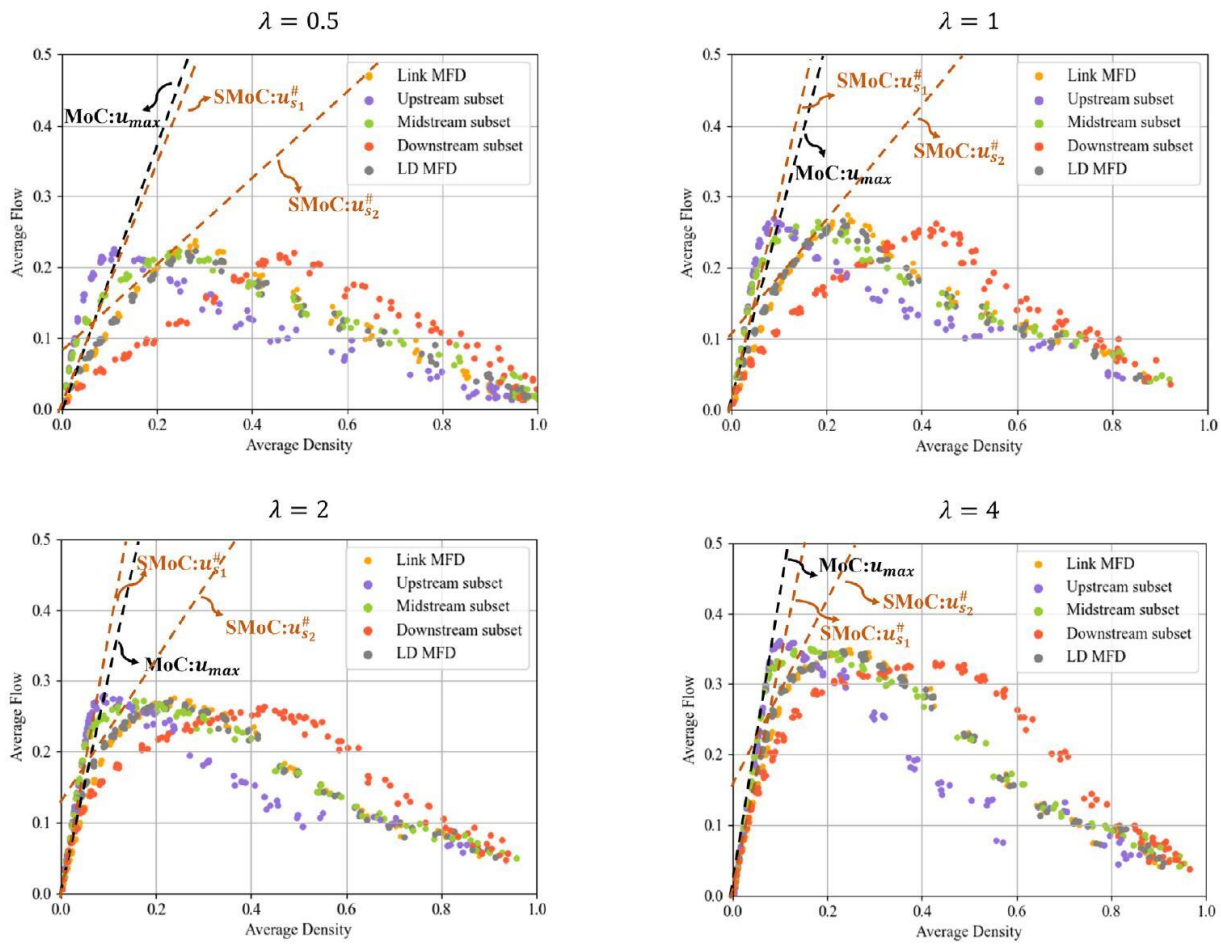

Fig 5 The link MFD, the LD-MFD, and the position-based subsets for different values of λ

5.0 CONCLUSION

This project presented an analysis of the impacts of loop detector position within the link on the resulting MFDs. Previous research has been based either on empirical data or simulation. Here, we have (i) added an analytical approach based on kinematic wave theory that enables the explanation of these impacts in the corridor MFD, (ii) postulated a logistic regression model based on empirical data to predict the occurrence of bias on a given network, and (iii) revealed that the network parameter λ plays a key role in the bias magnitude while the aggregation interval of the loop detector has no significant impact.

In the analytical approach, the symmetric triangular diagram on a corridor was used to envision and distinguish possible biases induced by the nature of loop detectors. Subject to the saturated initial condition constrained by the shock wave speed, the time-space diagram was classified according to the values of λ, ρ, and n. Formulae of the link MFD, LD-MFD, and the position-based subsets were cataloged. Several visualizations of MFDs and biases were presented. Under an ideal signalization, neither LD bias nor subset bias is apparent. If the

network is programmed for the first vehicle of the green time to arrive at the next intersection during the green time (e.g., $\lambda < 1$), the subset bias only depends on ρ. If the first vehicle arrives during the red time of the next intersection, the subset bias is subject to λ, ρ, and n. It was proved that the LD bias is inevitable unless the signal is programmed perfectly or red time is negligible or the loop detectors are uniformly distributed. Also, the possible range of LD-MFD can be obtained by the subset bias formulas presented here. If the subset bias is negligible, we can conclude that the LD-MFD is unbiased. However, if there is a significant subset bias, it is important to use caution when relying on the data as it may not accurately represent the traffic state at the network level. The analytical approach can be improved by considering an offset as an additional variable and identifying MFDs in unsaturated initial conditions. Also, other renowned FD models can be deployed to follow the same procedure.

Our simulation results indicated that the overlapping phenomenon described in the above paragraph can be explained by the network parameter λ. For short-block networks ($\lambda < 1$) we have seen that the different branches do not overlap and that they tend to overlap for very long-block networks ($\lambda \gg 1$). Although the empirical data does not include signal settings to verify these hypotheses, this finding highlights the importance of parameterizing urban networks according to their λ-value. Additionally, taking the benefits of simulation, we explored the effects of the aggregation interval, and we found that it is not a determining factor in any biases that may exist in the MFD.

6.0 RECOMMENDATIONS

The results of this paper strongly indicate that a correction method can be devised to improve the estimation of the link MFD using loop detector data. Overlapping position-based subset MFDs are fortunate to not require correction. However, when the subset bias is observed, LD-MFD may not accurately represent link MFD, which requires a correction method. As we have seen, both the topology of the network such as λ, and the distribution of positions should play a key role. This is currently being investigated by the authors.

7.0 REFERENCE LIST

1. Geroliminis, N., and Daganzo, C. F. (2008). "Existence of urban-scale macroscopic fundamental diagrams: Some experimental findings." Transportation Research Part B: Methodological 42 (9):759-770.
2. Leclercq, L., Chiabaut, N., and Trinquier, B. (2014). "Macroscopic fundamental diagrams: A cross-comparison of estimation methods." Transportation Research Part B: Methodological 62:1-12.
3. Buisson, C., and Ladier, C. (2009). "Exploring the impact of homogeneity of traffic measurements on the existence of macroscopic fundamental diagrams." Transportation Research Record 2124 (1):127-136.
4. Ambühl, L., Loder, A., Menendez, M., and Axhausen, K. W. (2017). "Empirical macroscopic fundamental diagrams: New insights from loop detector and floating car data." TRB 96th Annual Meeting Compendium of Papers.
5. Keyvan-Ekbatani, M., Papageorgiou, M., and Papamichail, I. (2013). "Urban congestion gating control based on reduced operational network fundamental diagrams." Transportation Research Part C: Emerging Technologies 33:74-87.
6. Loder, A., Ambühl, L., Menendez, M., and Axhausen, K. W. (2019). "Understanding traffic capacity of urban networks." Scientific reports 9 (1):1-10.
7. Greenshields, B.D., Bibbins, J.R., Channing, W., Miller, H.H., 1935. A study of traffic capacity.
8. Smeed, R.J., 1967. The road capacity of city centers. Highw. Res. Rec. (169).
9. Mahmassani, H.S., Williams, J.C., Herman, R., 1984. Investigation of network-level traffic flow relationships: some simulation results. Transp. Res. Rec. 971, 121–130. http://dx.doi.org/10.1177/036119818409700116.
10. Daganzo, C.F., Geroliminis, N., 2008. An analytical approximation for the macroscopic fundamental diagram of urban traffic. Transp. Res. B 42 (9), 771–781. http://dx.doi.org/10.1016/j.trb.2008.06.008.
11. Daganzo, C.F., 2005. A variational formulation of kinematic waves: Solution methods. Transp. Res. B 39 (10), 934–950. http://dx.doi.org/10.1016/j.trb.2004.12.002.
12. Geroliminis, N., Boyacı, B., 2012. The effect of variability of urban systems characteristics in the network capacity. Transp. Res. B 46 (10), 1607–1623. http://dx.doi.org/10.1016/j.trb.2012.08.001.
13. Laval, J.A., Castrillón, F., 2015. Stochastic approximations for the macroscopic fundamental diagram of urban networks. Transp. Res. Procedia 7, 615–630. http://dx.doi.org/10.1016/j.trb.2015.08.001.
14. Geroliminis, N., Sun, J., 2011a. Hysteresis phenomena of a Macroscopic Fundamental Diagram in freeway networks. Transp. Res. A 45, 966–979. http://dx.doi.org/10.1016/j.tra.2011.04.004.
15. Geroliminis, N., Sun, J., 2011b. Properties of a well-defined macroscopic fundamental diagram for urban traffic. Transp. Res. B 45 (3), 605–617. http://dx.doi.org/10.1016/j.trb.2010.11.004.
16. Zheng, N., Geroliminis, N., 2013. On the distribution of urban road space for multimodal congested networks. Procedia-Soc. Behav. Sci. 80, 119–138. http://dx.doi.org/10.1016/j.trb.2013.06.003.

17. Buisson, C., Ladier, C., 2009. Exploring the impact of homogeneity of traffic measurements on the existence of macroscopic fundamental diagrams. Transp. Res. Rec. 2124 (1), 127–136. http://dx.doi.org/10.3141/2124-12.
18. Yildirimoglu, M., Ramezani, M., Geroliminis, N., 2015. Equilibrium analysis and route guidance in large-scale networks with MFD dynamics. Transp. Res. Procedia 9, 185–204. http://dx.doi.org/10.1016/j.trpro.2015.07.011.
19. Ding, H., Guo, F., Zheng, X., Zhang, W., 2017. Traffic guidance–perimeter control coupled method for the congestion in a macro network. Transp. Res. C 81, 300–316. http://dx.doi.org/10.1016/j.trc.2017.06.010.
20. Gayah, V.V., Gao, X.S., Nagle, A.S., 2014. On the impacts of locally adaptive signal control on urban network stability and the macroscopic fundamental diagram. Transp. Res. B 70, 255–268. http://dx.doi.org/10.1016/j.trb.2014.09.010.
21. Huang, J., Hu, M.-B., Jiang, R., Li, M., 2018. Effect of pre-signals in a Manhattan-like urban traffic network. Physica A 503, 71–85. http://dx.doi.org/10.1016/j.physa.2018.02.170.
22. Zhang, L., Yuan, Z., Yang, L., Liu, Z., 2020. Recent developments in traffic flow modeling using macroscopic fundamental diagram. Transp. Rev. 40, 529–550. http://dx.doi.org/10.1080/01441647.2020.1738588.
23. Ji, Y., Luo, J., Geroliminis, N., 2014. Empirical observations of congestion propagation and dynamic partitioning with probe data for large-scale systems. Transp. Res. Rec. 2422 (1), 1–11. http://dx.doi.org/10.3141/2422-01.
24. Ambühl, L., Menendez, M., 2016. Data fusion algorithm for macroscopic fundamental diagram estimation. Transp. Res. C 71, 184–197. http://dx.doi.org/10.1016/j.trpro.2016.05.016.
25. Du, J., Rakha, H., Gayah, V.V., 2016. Deriving macroscopic fundamental diagrams from probe data: Issues and proposed solutions. Transp. Res. C 66, 136–149. http://dx.doi.org/10.1016/j.trb.2014.01.006.
26. An, K., Hu, X., Chen, X., 2020. Traffic network partitioning for hierarchical macroscopic fundamental diagram applications based on fusion of GPS probe and loop detector data. arXiv preprint arXiv:2011.09075.
27. Saffari, E., Yildirimoglu, M., Hickman, M., 2022. Data fusion for estimating Macroscopic Fundamental Diagram in large-scale urban networks. Transp. Res. C 137, 103555. http://dx.doi.org/10.1016/j.trc.2020.103012.
28. Kong, Q.-J., Li, Z., Chen, Y., Liu, Y., 2009b. An approach to urban traffic state estimation by fusing multisource information. IEEE Trans. Intell. Transp. Syst. 10 (3), 499–511. http://dx.doi.org/10.1109/TITS.2009.2026308.
29. Kim, E.-J., Kim, D.-K., Kho, S.-Y., Chung, K., 2020. Spatiotemporal filtering method for detecting kinematic waves in a connected environment. PLoS One 15 (12), e0244329. http://dx.doi.org/10.1371/journal.pone.0244329.
30. Min, J.H., Ham, S.W., Kim, D.-K., Lee, E.H., 2022. Deep multimodal learning for traffic speed estimation combining dedicated short-range communication and vehicle detection system data. Transp. Res. Rec. 03611981221130026. http://dx.doi.org/10.1177/03611981221130026.
31. Bramich, D., Menéndez, M., Ambühl, L., 2023. FitFun: A modelling framework for successfully capturing the functional form and noise of observed traffic flow–density–speed

relationships. Transp. Res. C Emerg. Technol. 151, 104068. http://dx.doi.org/10.1016/j.trc.2023.104068.
32. Barmpounakis, E., Geroliminis, N., 2020. On the new era of urban traffic monitoring with massive drone data: The pNEUMA large-scale field experiment. Transp. Res. C Emerg. Technol. 111, 50–71. http://dx.doi.org/10.1016/j.trc.2019.11.023.
33. Paipuri, M., Barmpounakis, E., Geroliminis, N., Leclercq, L., 2021. Empirical observations of multi-modal network-level models: Insights from the Pneuma experiment. Transp. Res. C 131, 103300. http://dx.doi.org/10.1016/j.trc.2021.103300.
34. FHWA, U., 2022. Traffic Control Systems Handbook: Chapter 6 Detectors - FHWA Office of Operations. URL https://ops.fhwa.dot.gov/publications/fhwahop06006/chapter_6.htm.
35. Hunt, P., Robertson, D., Bretherton, R., Winton, R., 1981. SCOOT-A Traffic Responsive Method of Coordinating Signals. Technical Report.
36. Sims, A.G., 1979. The Sydney coordinated adaptive traffic system. In: Engineering Foundation Conference on Research Directions in Computer Control of Urban Traffic Systems, 1979, Pacific Grove, California, USA.
37. Mirchandani, P., Head, L., 2001. A real-time traffic signal control system: architecture, algorithms, and analysis. Transp. Res. C 9 (6), 415–432. http://dx.doi.org/10.1016/S0968-090X(01)00023-0.
38. Kay, J., Henry, R.D., Smith, S., 1975. Locating Detectors for Advanced Traffic Control Strategies. Handbook. Technical Report.
39. Moore II, J.E., Jayakrishnan, R., McNally, M., MacCarley, C.A., 1999. SCOOT performance in anaheim advanced traffic control system. Intellimotion-Res. Updates Intell. Transp. Syst. 8 (3), http://dx.doi.org/10.3141/1644-01.
40. Kong, Q.-J., Chen, Y., Liu, Y., 2009a. A fusion-based system for road-network traffic state surveillance: a case study of Shanghai. IEEE Intell. Transp. Syst. Mag. 1 (1), 37–42. http://dx.doi.org/10.1109/MITS.2009.932719.
41. FDOT, 2016. Advanced signal control technology guidelines. URL https://ops.fhwa.dot.gov/publications/fhwahop06006/chapter_6.htm.
42. Buisson, C., Ladier, C., 2009. Exploring the impact of homogeneity of traffic measurements on the existence of macroscopic fundamental diagrams. Transp. Res. Rec. 2124 (1), 127–136. http://dx.doi.org/10.3141/2124-12.
43. Courbon, T., Leclercq, L., 2011. Cross-comparison of macroscopic fundamental diagram estimation methods. Procedia-Soc. Behav. Sci. 20, 417–426. http://dx.doi.org/10.1016/j.sbspro.2011.08.048.
44. Leclercq, L., Chiabaut, N., Trinquier, B., 2014. Macroscopic fundamental diagrams: A cross-comparison of estimation methods. Transp. Res. B 62, 1–12. http://dx.doi.org/10.1016/j.trb.2014.01.007.
45. Ambühl, L., Loder, A., Menendez, M., Axhausen, K.W., 2017. Empirical macroscopic fundamental diagrams: New insights from loop detector and floating car data. In: TRB 96th Annual Meeting Compendium of Papers. Transportation Research Board, pp. 17–03331. http://dx.doi.org/10.3929/ethz-b-000167171.
46. Edie, L.C., et al., 1963. Discussion of Traffic Stream Measurements and Definitions. Port of New York Authority New York, http://dx.doi.org/10.1016/B978-0-08-010439-0.50014-8.

47. Laval, J.A., Castrillón, F., 2015. Stochastic approximations for the macroscopic fundamental diagram of urban networks. Transp. Res. Procedia 7, 615–630. http://dx.doi.org/10.1016/j.trb.2015.08.001.
48. Laval, J.A., Chilukuri, B.R., 2016. Symmetries in the kinematic wave model and a parameter-free representation of traffic flow. Transp. Res. B 89, 168–177. http://dx.doi.org/10.1016/j.trb.2016.02.009.
49. Zhang, L., Garoni, T.M., de Gier, J., 2013. A comparative study of macroscopic fundamental diagrams of arterial road networks governed by adaptive traffic signal systems. Transp. Res. B 49, 1–23. http://dx.doi.org/10.1016/j.trb.2012.12.002.